Structure of Fast Ion Conductors $Li_{3x}La_{2/3-x}TiO_3$ Deduced from Powder Neutron Diffraction Experiments

A. Varez,[†] M. T. Fernández-Díaz,[‡] J. A. Alonso,[§] and J. Sanz*[,§]

Departamento de Materiales, Escuela Politécnica Superior, Universidad de Carlos III de Madrid, 28911 Leganés, Spain, Institut Laue-Langevin, F-38045, Grenoble, France, and Instituto Ciencia de Materiales, CSIC, Cantoblanco, E-28049, Madrid, Spain

Received December 10, 2004. Revised Manuscript Received February 22, 2005

High-temperature neutron diffraction (ND) experiments have been carried out in two representative members of the $Li_{3x}La_{2/3-x}TiO_3$ series ($x = 0.067$ and 0.167), to analyze the influence of temperature on the perovskite structure. In the orthorhombic Li-poor ordered member $Li_{0.2}La_{0.6}TiO_3$ (*Cmmm* space group), prepared by slowly cooling from 1673 K, the heating of the sample produced the elimination of the octahedral tilting along the *b*-axis ($a^0b^-c^0$ scheme) at 873 K, requiring higher temperatures to induce the vacancies disordering. In the rhombohedral Li-rich disordered member $Li_{0.5}La_{0.5}TiO_3$ ($R\bar{3}c$ space group), prepared by quenching from 1673 K, the sample heating produced the elimination of the octahedral tilting along the [111] direction ($a^-a^-a^-$ scheme) at 1073 K. The elimination of octahedral tilting drived the orthorhombic−tetragonal transformation in the first perovskite and the rhombohedral−cubic transformation in the second perovskite. A detailed analysis of four identified phases showed that distortions of LaO_{12} cubooctahedra depends on the octahedral tilting and on the vacancy distribution adopted by the perovskite. Finally, the influence of these two parameters, octahedral tilting and vacancy ordering, on the Li mobility of the perovskite series has been discussed.

Introduction

Since the discovery of the high ionic conductivity in the $Li_{3x}La_{2/3-x}TiO_3$ series,[1,2] with perovskite structure (LLTO), this system has attracted the interest of many research groups because of its potential application as a solid electrolyte in electrochemical devices.[3] The aim of many of these works was to identify structural features that enhance lithium mobility in these compounds ($\sigma \approx 10^{-2}$ S·cm^{-1} at 300 K).[1,2,4−8] In these perovskites, La^{3+} ions can be substituted by Li^+ ions, and the amount of nominal vacant A-sites is given by $\square = 1/3-2x$. In orthorhombic Li-poor perovskites, $x < 0.1$, the ordering of vacancies in alternated planes favors the mobility of Li ions in layers perpendicular to the *c*-axis.[7−9] In samples with higher Li contents, $x > 0.1$, ordering decreases and symmetry becomes tetragonal.[6,7]

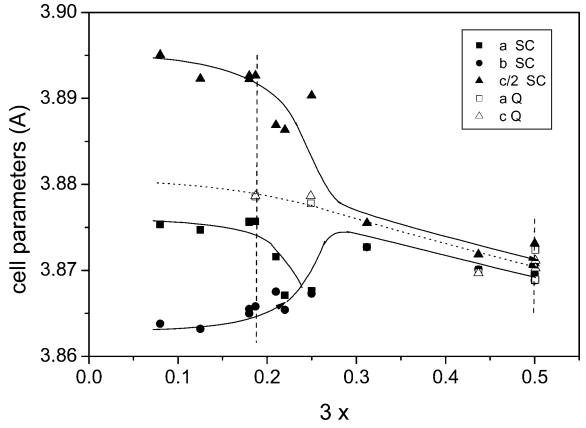

Figure 1. Lattice parameters versus Li content in $Li_{3x}La_{2/3-x}TiO_3$ perovskites deduced from XRD experiments (adapted from refs 8 and 20). In slowly cooled samples (close symbols) the structure changes from orthorhombic to tetragonal for *x* values near 0.08. In the case of quenched samples (open symbols) the pseudocubic symmetry is predominant in the compositional range analyzed.

Finally in cubic Li-rich samples, quenched from high temperature,[8,10−12] vacancy ordering was removed and Li mobility displayed a three-dimensional character.

The knowledge of structural features is crucial to understanding Li mobility within the La−Ti−O framework. In particular, tilting of TiO_6 octahedra is an important feature that introduces structural distortions in square windows that connect contiguous A-sites, affecting Li mobility along the

* To whom correspondence should be addressed. E-mail: jsanz@icmm.csic.es.
† Universidad de Carlos III de Madrid.
‡ Institut Laue-Langevin.
§ Instituto Ciencia de Materiales, CSIC.

(1) Belous, A. G.; Novitskaya, G. N.; Polyanetskaya, S. V.; Gornikov, Y. I. *Zh. Neorg. Khim.* **1987**, *32*, 283.
(2) Inaguma, Y.; Chen, L.; Itoh, M.; Nakamura, T.; Uchida, T.; Ikuta, H.; Wakihara, M. *Solid State Commun.* **1993**, *86*, 689.
(3) Stramare, S.; Thangadurai, V.; Weppner, W. *Chem. Mater.* **2003**, *15* (21), 3974.
(4) Kawai, H.; Kuwano, J. *J. Electrochem. Soc.* **1994**, *141*, L78.
(5) Robertson, A. D.; García-Martín, S.; Coats, A.; West, A. R. *J. Mater. Chem.* **1995**, *5*, 1405.
(6) Fourquet, J. L.; Duroy, H.; Crosnier-Lopez, M. P. *J. Solid State Chem.* **1996**, *127*, 283.
(7) Ruiz, A. I.; López, M. L.; Veiga, M. L.; Pico, C. *Solid State Ionics* **1998**, *112*, 291.
(8) Ibarra, J.; Várez, A.; León, C.; Santamaría, J.; Torres-Martinez, L. M.; Sanz, J. *Solid State Ionics* **2000**, *134*, 219.
(9) Paris, M. A.; Sanz, J.; Leon, C.; Santamaría, J.; Ibarra, J.; Varez, A. *Chem. Mater.* **2000**, *12*, 1694.
(10) Inaguma, Y.; Yu, J. D.; Katsumata, T.; Itoh, M. *J. Ceram. Soc. Jpn. Int. Ed.* **1997**, *105* (6), 548.
(11) Harada, Y.; Hirakoso, Y.; Kawai, H.; Kuwano, J. *Solid State Ionics* **1999**, *121*, 245.
(12) Mazza, D.; Roncheti, S.; Bohnké, O.; Duroy, H.; Fourquet, J. L. *Solid State Ionics* **2002**, *149*, 81.

10.1021/cm047841f CCC: $30.25
Published on Web 04/09/2005

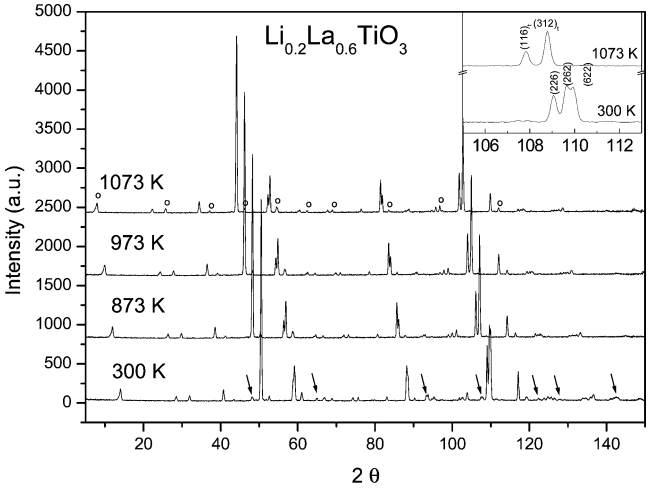

Figure 2. ND patterns of $Li_{0.2}La_{0.6}TiO_3$ perovskite heated at 300, 873, 973, and 1073 K. The main peaks are indexed with the basic perovskite cell. Superstructure peaks denoted with open circles (○) arise from cation/vacancy ordering in A-sites of the perovskite, while the peaks indicated with arrows emerge as a consequence of the TiO_6 tilting. Inset illustrates the orthorhombic−tetragonal transition produced as temperature increases.

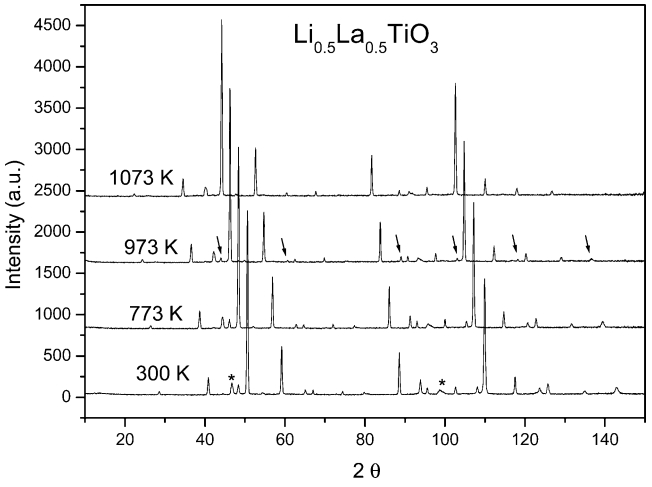

Figure 3. ND patterns of $Li_{0.5}La_{0.5}TiO_3$ perovskite heated at 300, 773, 973, and 1073 K. Arrows denote the superstructure peaks associated with the TiO_6 tilting. Small peaks marked with asterisks correspond to the most intense reflections of a secondary phase which do not disappear during thermal treatments.

three orthogonal directions of the perovskite. However, a determination of octahedral tilting by X-ray diffraction is particularly difficult because superlattice reflections produced by tilting of TiO_6 octahedra arise from the oxygen atoms, which are weak scatterers if compared with La and Ti atoms. Hence, neutron diffraction (ND) measurements are more suitable for this investigation.

In recent works, neutron diffraction experiments were carried out at room temperature to determine structural features of the Li-poor $La_{0.12}La_{0.63}TiO_3$ perovskite, described with orthorhombic symmetry (*Cm*2*m* and *Cmmm* space groups),[13−15] and the Li-rich $La_{0.5}Li_{0.5}TiO_3$ perovskite, described with the rhombohedral model ($R\bar{3}c$ space group).[16]

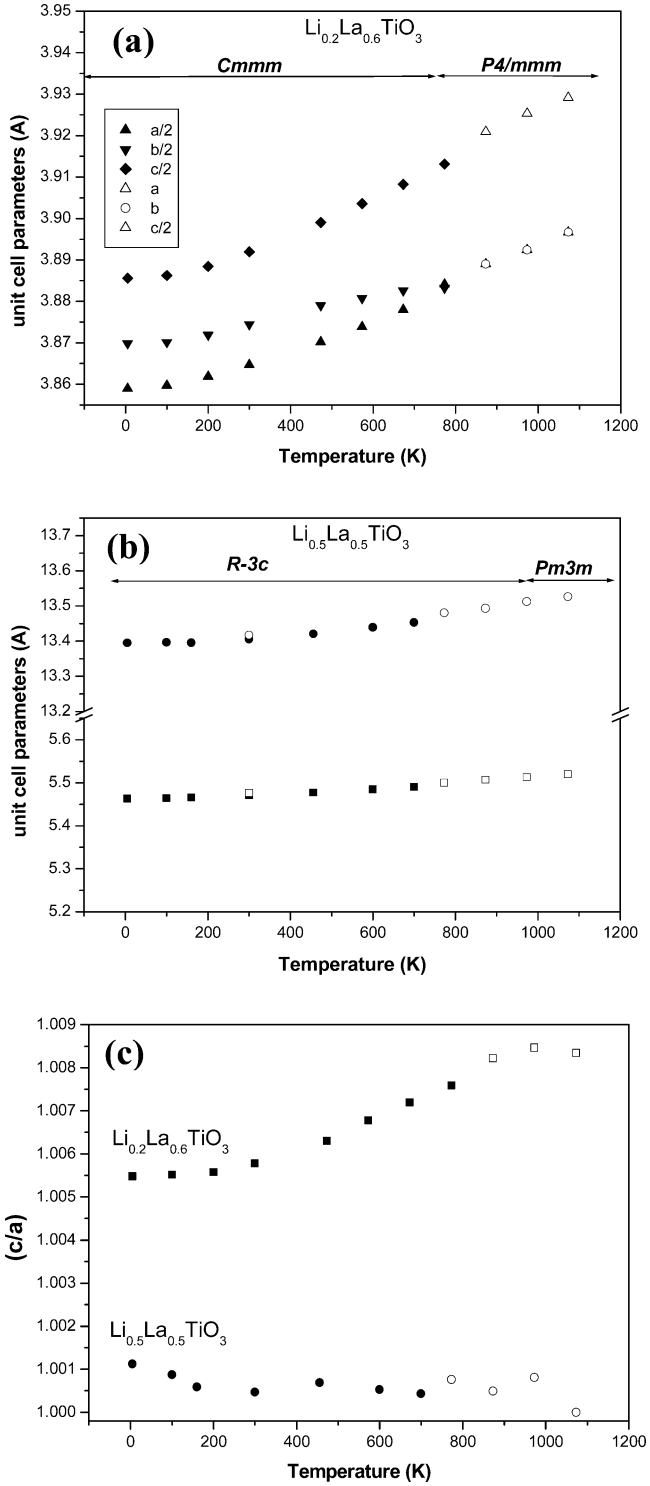

Figure 4. Temperature dependence of unit cell parameters in (a) $Li_{0.2}La_{0.6}TiO_3$ and (b) $Li_{0.5}La_{0.5}TiO_3$ perovskites, and (c) temperature dependence of c/a ratios of the two perovskites. Open and closed symbols correspond to experimental data recorded in D1A and D2B diffractometers. Lattice parameters of unit cells have been divided by appropiated factors to be compared with those of the single cubic perovskite.

In the orthorhombic perovskite, it was shown that the distortion of TiO_6 octahedra was produced by distribution of vacancies in alternated planes along the *c*-axis. In the rhombohedral phase, octahedra are regular and distribution of vacancies is disordered. As a consequence of the different

(13) Sanz, J.; Alonso, J. A.; Várez, A.; Fernández-Díaz, M. T. *Dalton Trans.* **2002**, 1406.
(14) Inaguma, Y.; Katsumata, T.; Itoh, M.; Morii, Y. *J. Solid. State Chem.* **2002**, *166*, 67.
(15) Varez, A.; Inaguma, Y.; Fernández-Díaz, M. T.; Alonso, J. A.; Sanz, J. *Chem. Mater.* **2003**, *15* (24), 4637.
(16) Alonso, J. A.; Sanz, J.; Santamaría, J.; León, C.; Varez, A.; Fernandez-Diaz, M. T. *Angew. Chem., Int. Ed.* **2000**, *3*, 619.

Table 1. Positional Parameters for the Rhombohedral, Cubic, Orthorhombic, and Tetragonal Perovskites Used in Structural Refinements

Space Group $R\bar{3}c$ (No. 167)			Space Group $Pm3m$ (No. 221)			Space Group $Cmmm$ (No. 65)			Space Group $P4/mmm$ (No. 123)		
atom	sites	atomic coordinates	atom	sites	atomic coordinates	atom	sites	atomic coordinates	atom	sites	atomic coordinates
La	6 a	$0,0,^1/_4$	La	1 b	$^1/_2,^1/_2,^1/_2$	La1	4 i	$0,y \approx ^1/_4,0$	La1	1 a	0,0,0
Li	18 d	$^1/_2,0,0$	Li	3 c	$^1/_2,^1/_2,0$	La2	4 j	$0,y \approx ^1/_4,^1/_2$	La2	1 b	$0,0,^1/_2$
Ti	6 b	0,0,0	Ti	1 a	0,0,0	Ti	8 o	$x \approx ^1/_4,0,z \approx ^1/_4$	Ti	2 h	$^1/_2,^1/_2,z$
O	18 e	$x \approx ^1/_2,0,^1/_4$	O	3 d	$^1/_2,0,0$	O1	4 g	$x \approx ^1/4,0,0$	OI	1 c	$^1/_2,^1/_2,0$
						O2	4 k	$0,0,z \approx ^1/_4$	OII	4 i	$0,^1/_2,z$
						O3	4 l	$0,^1/_2,z \approx ^1/_4$	OIII	1 d	$^1/_2,^1/_2,^1/_2$
						O4	8 m	$^1/_4,^1/_4, z \approx ^1/_4$			
						O5	4 h	$x \approx ^1/_4, 0,^1/_2$			

distribution of vacancies, octahedral tilting schemes detected in two perovskites were different. A detailed analysis of Fourier map differences showed that Li cations, in both pervoskites, occupy the center of the unit cell faces, making changes on symmetry and dimensions of the unit cell affect the distribution and mobility of lithium in perovskites.[14−16]

In this work, structural changes produced during heating of $Li_{3x}La_{2/3-x}TiO_3$ perovskites with $x = 0.067$ and 0.16 have been analyzed with neutron diffraction technique. The choice of these two compositions was oriented to the preparation of the ordered and disordered end members of the series; for that, the first perovskite was slowly cooled and the second perovskite was quenched into liquid nitrogen from high temperature. In this analysis, modifications on octahedral tilting and ordering of La-vacancies have been analyzed as a function of temperature. From the structural information obtained, some characteristics of Li mobility have been deduced.

Experimental Section

Sample Preparation. $Li_{0.2}La_{0.6}TiO_3$ and $Li_{0.5}La_{0.5}TiO_3$ perovskites have been prepared from stoichiometric amounts of Li_2CO_3, La_2O_3, and TiO_2 (high-purity grade), following the procedure described elsewhere.[2,8] To reduce the absorption cross section in neutron diffraction experiments, a ^{7}Li enriched reagent was used. Stoichiometric mixtures were ground in an agate mortar with acetone and calcined in air for 4 h at 800 °C. Calcined powders were reground, pressed into pellets under a pressure of 500 kg/cm^2 (50 MPa), and heated at 1150 °C. The pellets were finally heated at 1350 °C; from this temperature, $Li_{0.2}La_{0.6}TiO_3$ was slowly cooled (1 °/min) to room temperature, and $Li_{0.5}La_{0.5}TiO_3$ was quenched into liquid nitrogen. Inductively coupled plasma spectroscopy (ICP), using a JY-70 plus spectrometer, was used to evaluate the metal molar ratio. In all cases, chemical data obtained conformed to nominal compositions.

X-ray powder patterns were collected at room temperature in a Phillips X-pert diffractometer with ($\theta/2\theta$) Bragg−Brentano geometry using the Cu Kα radiation ($\lambda = 1.5418$ Å). For phase assessment and indexing purposes, data were recorded between $2\theta = 5$ and 90°.

ND patterns were collected in two high-resolution powder diffractometers of ILL (Grenoble, France). From 5 to 300 K, the D2B (1.954 Å) instrument was used, whereas for high-temperature experiments, 300−1073 K, the D1A instrument was chosen (1.912 Å). In both apparatus, the wavelength was selected with a Ge monochromator. ND patterns were recorded, using 4 g of sample contained in a vanadium can. In a first step, ND patterns were indexed with the Treor program. Structural analysis was carried out with the Rietveld method (Fullprof program),[17] for that, a pseudo-Voigt function was chosen to reproduce the line shape of diffraction peaks. In this analysis, coherent scattering lengths used for La, Li, Na, Ti, and O were 8.24, −1.90, 3.63, −3.30, and 5.80 fm, respectively.

Results

XRD Analysis. In LLTO perovskites, vacancy ordering governs most of the structural features. In samples with low Li content, the vacancy ordering is favored, however, in samples with high Li content, the cation disordering prevailed. In Figure 1, evolution of unit cell parameters of slowly cooled and quenched samples, expressed in terms of the ideal cubic perovskite, are given as a function of the lithium content. From the structural point of view, two extreme samples can be distinguished: the slowly cooled $Li_{0.2}La_{0.6}TiO_3$ (ordered, with $c/2a > 1$) and the quenched $Li_{0.5}La_{0.5}TiO_3$ (disordered with $c/2a \approx 1$) samples. The choice of both compositions was oriented to the preparation of the ordered and disordered end members of the series.

XRD pattern of the slowly cooled $Li_{0.2}La_{0.6}TiO_3$ was interpreted on the basis of an orthorhombic doubled perovskite ($a_p,a_p,2a_p$) (*Pmmm* space group),[8−10] and that of the quenched $Li_{0.5}La_{0.5}TiO_3$ sample was fitted with a single cubic perovskite model (a_p,a_p,a_p, *Pm*3*m* space group).[5,8,11] In intermediate compositions, width and intensity of superstructure peaks are strongly dependent on Li contents and cooling rates,[5,6,18] making structural analyses difficult.

ND Analysis. Figures 2 and 3 show ND patterns of $Li_{0.2}La_{0.6}TiO_3$ and $Li_{0.5}La_{0.5}TiO_3$ perovskites recorded at increasing temperatures between 300 and 1073 K. In Figure 4, the temperature dependence of unit cell parameters of the two samples is given. In this figure, low-temperature data deduced previously in samples with similar compositions have been included.[19]

ND patterns of the slowly cooled $Li_{0.2}La_{0.6}TiO_3$ sample, recorded at increasing temperatures, were refined considering an orthorhombic doubled $2a_p,2a_p,2a_p$ model (*Cmmm* space group), with parameters $a \approx 7.73$ Å, $b \approx 7.75$ Å, $c \approx 7.79$

(17) Rodriguez-Carvajal, J. FULLPROF: A Program for Rietveld Refinement and Pattern Matching Analysis. In *Abstracts of the Satellite Meeting on Powder Diffraction of the XV Congress of the IUCr*; International Union of Crystallography: Toulouse, France, 1990; p. 127.
(18) García-Martín, S.; Alario-Franco, M. A.; Ehrenberg, H.; Rodríguez-Carvajal, J.; Amador, U. *J. Am. Chem. Soc.* **2004**, *126* (11), 3587.
(19) Sanz, J.; Várez, A.; Alonso, J. A.; Fernández-Díaz, M. T.. *J. Solid State Chem.* **2004**, *177*, 1157.

Table 2. Structural Parameters of $Li_{0.2}La_{0.6}TiO_3$ and $Li_{0.5}La_{0.5}TiO_3$ Deduced from Neutron Diffraction Data Taken between 5 and 1073 K

Part A: $Li_{0.2}La_{0.6}TiO_3$ [a]

atom	param.	5 K	100 K	200 K	300 K	370 K	473 K	573 K	673 K	773 K	873 K (T)	973 K (T)	1073 K (T)	parameter	atom
La1	*y*	0.2555(4)	0.2557(3)	0.2545(6)	0.2546(5)	0.2542(6)	0.2539(6)	0.2543(3)	0.2519(8)	0.2521(9)					
	B	0.28(3)	0.38(3)	0.63(4)	0.61(3)	0.82(4)	0.93(4)	1.00(4)	1.15(4)	1.25(4)	1.30(14)	1.50(10)	1.60(11)	B	La1
	occ	0.966(5)	0.965(6)	0.968(6)	0.969(5)	0.983(6)	0.971(5)	0.957(5)	0.964(5)	0.963(6)	0.93(1)	0.93(1)	0.93(1)	occ	
La2	*y*	0.2621(15)	0.2620(15)	0.2617(21)	0.2616(17)	0.2608(23)	0.2591(23)	0.2598(19)	0.2560(32)	0.2590(31)					
	B	0.29(14)	0.32(15)	0.66(18)	0.60(15)	0.87(19)	0.87(16)	0.91(15)	1.11(16)	1.24(20)	1.30(14)	1.60(10)	1.60(10)	B	La2
	occ	0.244(4)	0.238(5)	0.236(5)	0.245(4)	0.235(5)	0.241(4)	0.239(4)	0.241(5)	0.241(5)	0.24(1)	0.24(1)	0.25(1)	occ	
Ti	*x*	0.2477(10)	0.2486(10)	0.2479(12)	0.2477(11)	0.2489(13)	0.2485(12)	0.2489(12)	0.2482(12)	0.2486(9)					
	z	0.2599(4)	0.2596(4)	0.2602(4)	0.2601(4)	0.2606(4)	0.2597(4)	0.2602(4)	0.2605(4)	0.2608(4)	0.2619(9)	0.2611(9)	0.2610(10)	z	Ti
	B	0.37(3)	0.41(3)	0.59(4)	0.55(3)	0.56(4)	0.80(4)	0.87(4)	0.98(4)	1.11(4)	1.14(13)	1.20(9)	1.30(9)	B	
O1	*x*	0.2724(5)	0.2715(5)	0.2712(6)	0.2710(6)	0.2698(7)	0.2676(7)	0.2651(8)	0.2605(10)	0.2525(10)					(OI)
	B	0.87 (6)	0.91(6)	1.01(7)	1.23(6)	1.03(7)	1.54(7)	1.74(7)	2.11(7)	2.38(7)	2.30(20)	2.63(20)	2.66(20)	B	
O2	*z*	0.2139(4)	0.2137(4)	0.2141(5)	0.2139(4)	0.2136(5)	0.2168(5)	0.2186(6)	0.2197(7)	0.2200 (8)					
	B	0.62(6)	0.66(6)	0.91(7)	0.75(6)	0.97(7)	1.11(8)	1.31(8)	1.48(12)	1.47(14)					
O3	*z*	0.2612(4)	0.2613(4)	0.2600(5)	0.2592(5)	0.2592(5)	0.2574(5)	0.2569(6)	0.2527(9)	0.2456(11)	0.2361(6)	0.2365(7)	0.2373(7)	z	(OII)
	B	0.94(7)	0.89(7)	0.96(8)	1.12(7)	1.21(8)	1.35(9)	1.66(10)	1.82(13)	1.91(18)	2.07(9)	2.19(17)	2.35(16)	B	
O4	*z*	0.2329(4)	0.2333(4)	0.2337(4)	0.2341(4)	0.2356(4)	0.2342(5)	0.2346(6)	0.2357(9)	0.2387(10)					
	B	1.02(4)	1.03(4)	1.10(5)	1.17(4)	1.11(4)	1.56(5)	1.70(5)	1.88(7)	2.18(14)					
O5	*x*	0.2314(6)	0.2311(6)	0.2328(7)	0.2304(6)	0.2311(7)	0.2296(7)	0.2300(8)	0.2297(9)	0.2307(9)					
	B	1.06(6)	1.21(6)	1.31(7)	1.27(6)	1.37(7)	1.54(7)	1.93(8)	1.98(9)	2.08(9)	2.52(20)	2.67(13)	2.81(14)	B	(OIII)
a(Å)		7.7180(1)	7.7194(1)	7.7238(1)	7.7294(1)	7.7317(1)	7.7404(1)	7.7478(1)	7.7561(2)	7.7683(6)	3.8890(1)	3.8924(1)	3.8967(1)		
b(Å)		7.7397(1)	7.7403(1)	7.7438(1)	7.7489(1)	7.7512(1)	7.7580(1)	7.7615(1)	7.7652(2)	7.7664(6)	3.8890(1)	3.8924(1)	3.8967(1)		
c(Å)		7.7713(1)	7.7725(1)	7.7769(1)	7.7839(1)	7.7875(1)	7.7981(1)	7.8072(1)	7.8165(1)	7.8263(1)	7.8419(2)	7.8507(2)	7.8584(3)		
V(Å^3)		464.22(1)	464.41(1)	465.15(1)	466.21(1)	466.70(1)	468.28(1)	469.48(1)	470.77(2)	472.17(5)	118.605(5)	118.95(1)	119.32(1)		
$(c/a)_{normal}$		1.00549	1.00552	1.00557	1.00578	1.00595	1.00631	1.00678	1.00720	1.00759	1.00822	1.00847	1.00834		
R_I		6.94	7.23	8.40	6.41	7.25	5.95	6.12	6.44	6.30	8.08	7.64	8.65	R_I	
R_F		7.73	7.84	8.81	6.75	8.03	7.75	9.76	10.2	9.12	10.2	10.40	12.6	R_F	
R_P		5.12	5.29	5.69	5.03	5.08	4.88	4.61	4.76	4.90	7.67	7.88	8.37	R_P	
R_{WP}		7.16	7.38	7.76	7.10	7.29	6.69	6.43	6.79	6.69	10.4	10.07	11.5	R_{WP}	
R_{exp}		2.67	2.67	2.66	2.57	2.66	3.63	3.16	3.17	3.18	5.24	5.31	5.30	R_{exp}	
χ^2		7.18	7.62	8.50	7.64	7.53	3.39	4.11	4.58	4.39	2.31	2.65	3.31	χ^2	

Part B: $Li_{0.5}La_{0.5}TiO_3$ [b]

atom	param.	5 K	100 K	160 K	300 K	456 K	600 K	700 K	773 K	873 K	973 K	1073 K (C)	parameter
La	*B*	0.73(14)	0.72(13)	0.71 (7)	0.70(18)	0.77(14)	0.83(8)	0.94(10)	0.92(21)	1.00(21)	1.08(15)	1.16(15)	*B*
	occ	0.552(4)	0.546(3)	0.537 (2)	0.495(4)	0.516(4)	0.516 (2)	0.513(2)	0.495(4)	0.504(4)	0.498(4)	0.492(6)	*occ*
Li	*B*	5.19(99)	5.58(99)	8.03 (99)	16.56(99)	11.93(99)	28.30(99)	20.43(99)	29.20(99)	39.90(99)	41.00(99)	40.30(99)	*B*
	occ	0.149(4)	0.151 (3)	0.154(2)	0.168(4)	0.161(4)	0.161 (2)	0.163(3)	0.163(4)	0.166(4)	0.162(4)	0.167(6)	*occ*
Ti	*B*	1.06(18)	1.19(19)	1.20 (7)	1.20(21)	1.30(15)	1.39(8)	1.53(9)	1.46(21)	1.53(20)	1.64(4)	1.62(4)	*B*
O1	*x*	0.5313(8)	0.5300(6)	0.5296(4)	0.5327(7)	0.5319(8)	0.5327(4)	0.5296(6)	0.5301(8)	0.5262(10)	0.520(8)		*x*
	B[c]	1.64(10)	1.75(11)	1.80(12)	1.68(11)	2.00(13)	2.06(10)	2.32(12)	2.64(11)	2.98(10)	3.23(10)	3.63(12)	*B*
a (Å)		5.4631(3)	5.4633(3)	5.4660(3)	5.4756 (5)	5.4772(5)	5.4850(3)	5.4909(4)	5.50001(9)	5.5069 (1)	5.5129(1)	3.9036 (2)	*a* (Å)
c (Å)		13.394(3)	13.391(2)	13.395(1)	13.417 (3)	13.420(3)	13.440(1)	13.453(2)	13.480 (1)	13.493 (1)	13.512(2)		*c* (Å)
V (Å^3)		346.19(7)	346.15(7)	346.59(4)	348.39 (9)	348.66(8)	350.18(4)	351.28(4)	353.15 (4)	354.37 (4)	355.63(6)	59.486(5)	*V* (Å^3)
$(c/a)_{normal}$		1.00093	1.00067	1.00039	1.00027	1.00049	1.00030	1.00031	1.00058	1.00029	1.00061	1	c/a
R_I		7.44	7.42	4.06	5.75	4.31	2.70	3.79	3.20	3.20	2.54	1.46	R_I
R_F		6.13	6.94	4.00	5.44	4.24	2.65	3.46	2.29	2.54	2.28	1.21	R_F
R_P		9.05	6.84	4.82	7.67	8.62	4.72	4.69	5.51	5.31	4.89	5.21	R_P
R_{WP}		12.7	9.46	6.38	10.8	11.4	6.21	6.49	7.88	7.67	7.13	7.67	R_{WP}
R_{exp}		3.05	2.61	2.37	4.23	3.99	2.91	2.96	4.15	4.19	4.24	3.70	R_{exp}
χ^2		5.94	5.23	3.25	2.30	3.03	2.38	2.94	2.24	2.32	2.42	2.68	χ^2

[a] Below 873 K a $2a_p x 2a_p x 2a_p$ (*Cmmm* space group) unit cell was used. Above 873 K the best structural model was tetragonal with $a_p x a_p x 2a_p$ (*P*4/*mmm* space group). Data from 5 to 773 K were taken from ref 19. [b] Using the rhombohedral model ($R\bar{3}c$ space group). At the highest temperature, the cubic *Pm*3*m* model is used. [c] $B_{equi} = {}^4/_3\{a_1{}^*a_1{}^*\beta_{11} + a_2{}^*a_2{}^*\beta_{22} + c^*c^*\beta_{33} + 2a_1{}^*a_2{}^*\beta_{12} + a_1{}^*c^*\beta_{13} + a_2{}^*c^*\beta_{23}\}$.

Table 3. Temperature Dependence of Ti−O and La−O Distances and Tilt Angle (φ (deg)) for $Li_{0.2}La_{0.6}TiO_3$ (Distances Are Given in Å and Angles are Given in Degrees)[a]

	5 K	100 K	200 K	300 K	370 K	473 K	573 K	673 K	773 K	873 K	973 K	1073 K	
Ti−O1	2.028	2.028	2.033	2.031	2.033	2.032	2.035	2.036	2.040	2.042	2.056	2.052	Ti−OI
Ti−O2	1.949	1.953	1.951	1.959	1.957	1.954	1.955	1.936	1.943				
Ti−O3	1.943	1.941	1.945	1.940	1.942	1.945	1.945	1.960	1.960	1.952	1.957	1.957	Ti−OII
Ti−O4	1.946	1.946	1.947	1.948	1.947	1.950	1.950	1.950	1.951				
Ti−O5	1.871	1.870	1.869	1.874	1.872	1.878	1.878	1.875	1.873	1.871	1.869	1.877	Ti−OIII
φ (deg)	4.7	4.6	4.6	4.6	4.5	4.5	3.9	3.4	2.4	0	0	0	
La1−O1	2.862	2.866	2.874	2.881	2.870	2.850	2.862	2.788	2.758	2.750	2.753	2.755	La1−OI
La1−O1′	2.622	2.605	2.599	2.594	2.607	2.632	2.622	2.700	2.735				
La1−O2	2.624	2.550	2.567	2.582	2.578	2.588	2.624	2.603	2.648	2.687	2.688	2.693	La1−OII
La1−O3	2.756	2.806	2.789	2.775	2.776	2.779	2.756	2.768	2.761				
La1−O4	2.668	2.650	2.653	2.655	2.665	2.662	2.668	2.670	2.654				
La2−O2	2.972	2.951	2.961	3.031	3.009	2.969	2.974	2.958	2.894	2.837	2.842	2.843	La2−OII
La2−O3	2.656	2.679	2.675	2.610	2.638	2.676	2.667	2.698	2.728				
La2−O4	2.828	2.830	2.830	2.835	2.825	2.835	2.835	2.839	2.864				
La2−O5	2.664	2.642	2.666	2.721	2.698	2.657	2.688	2.652	2.648	2.750	2.752	2.755	La2−OIII
La2−O5′	2.806	2.826	2.806	2.765	2.785	2.831	2.804	2.846	2.852				

[a] Data from 5 to 773 K were taken from ref 19.

Table 4. Evolution with Temperature of the Ti−O and La−O distances (in Å) and octahedral tilt angles, φ, (in Degrees) (Diagonal O−O Distances of Square Windows Relating Contiguous A-Sites are Indicated)

	5 K	100 K	160K	300 K	456 K	600 K	700 K	773 K	873 K	973 K	1073 K (C)	
Ti−O	1.940	1.940	1.941	1.948	1.942	1.947	1.948	1.952	1.951	1.953	1.952	Ti−O
<La−O>	2.735	2.735	2.736	2.742	2.739	2.745	2.748	2.753	2.755	2.758	2.760	La−O
3*x*La−O′	2.560	2.564	2.556	2.520	2.570	2.564	2.581	2.585	2.627	2.644		3*x*La−O′
6*x*La−O	2.739	2.739	2.740	2.747	2.742	2.749	2.751	2.756	2.757	2.760	2.760	6*x*La−O
3*x*La−O″	2.903	2.900	2.910	2.956	2.903	2.920	2.909	2.915	2.879	2.869		3*x*La−O″
τ[a]	0.9971	0.9972	0.9969	0.9968	0.9970	0.9969	0.9974	0.9973	0.9984	0.9988	1.0000	*t*
φ (deg)	5.06	4.88	4.75	5.11	4.90	5.23	4.79	4.70	4.24	1.62	0	φ (deg)
(O−O)l	4.114	4.109	4.123	4.131	4.123	4.138	4.121	4.131	4.103	3.977	3.909	(O−O)l
(O−O)s	3.630	3.635	3.624	3.623	3.639	3.636	3.658	3.636	3.696	3.822	3.909	(O−O)s

[a] τ = Goldschmidt tolerance factor= $d_{A-O}/\sqrt{2}d_{B-O}$.

Å[13,14,19] (see Table 2, part a). From 5 to 300 K, ND patterns do not change in a significant way; however, above 600 K, some doublets merged into single peaks (i.e., (200)/(020); (044)/(404); (262)/(622)) and some peaks decreased in intensity, disappearing at 873 K (arrows in Figure 2). Both facts confirm the orthorhombic−tetragonal transition detected in XRD[9,20] and ND[19] experiments. The ND patterns of the sample heated above 873 K were indexed with a doubled a_p,a_p,$2a_p$ unit cell (*P*4/*mmm* space group).[9,20]

In the case of the quenched $Li_{0.5}La_{0.5}TiO_3$ perovskite, the room-temperature ND pattern was indexed with the rhombohedral $\sqrt{2}a_p$,$\sqrt{2}a_p$,$2\sqrt{3}a_p$ unit cell ($R\bar{3}c$ space group), with parameters $a \approx 5.476$ Å and $c \approx 13.417$ Å[16] (see Table 2, part b). In this pattern, peaks labeled with asterisks correspond to a residual non-identified impurity that does not change with temperature (see Figure 3). Superstructure peaks associated with the tilting of octahedra (arrows in Figure 3) decrease progressively with temperature, disappearing above 1073 K. Above this temperature, the ND pattern was indexed with the simple cubic a_p,a_p,a_p unit cell of the perovskite (*Pm*3*m* space group).

In the slowly cooled $Li_{0.2}La_{0.6}TiO_3$ perovskite, the orthorhombic−tetragonal transition has been observed at temperatures close to 773 K.[9,19,20] In the temperature range 5−300 K lattice parameters increase smoothly, whereas above 300 K unit cell expansion becomes more important (Figure 4a). In the case of the quenched $Li_{0.5}La_{0.5}TiO_3$ sample, three regimes were identified. Up to 300 K the thermal expansion of the unit cell is small. From room temperature to 973 K, unit cell parameters increase considerably. Finally, at higher temperatures a new regime was detected in which the unit cell expansion was again moderate (Figure 4b).

Comparing results obtained in both samples, it can be concluded that the disordered rhombohedral sample displays a smaller and more isotropic expansion than the ordered orthorhombic sample. The temperature dependence of *c*/*a* ratio is given in Figure 4c. In the orthorhombic sample, *c*/2*a* values remain basically constant below 300 K, but increase above this temperature, decreasing slowly above 1000 K. In the rhombohedral sample, the normalized *c*/*a* ratio decreases monotonically toward 1 as the temperature increases.

ND Rietveld Analysis. The Rietveld analysis of ND patterns of $Li_{0.2}La_{0.6}TiO_3$ and $Li_{0.5}La_{0.5}TiO_3$ perovskites was carried out with the Fullprof program using structural models given in Table 1. Structural parameters and interatomic distances deduced in this analysis are given in Tables 2−4. In all analyzed cases, thermal factors are reasonable and sites-occupancies agree with composition of samples.

1. Orthorhombic−Tetragonal Transformation. In the orthorhombic $2a_p$,$2a_p$,$2a_p$ phase of the $Li_{0.2}La_{0.6}TiO_3$ perovskite (*Cmmm* space group), La ions preferentially occupy La1 sites at $z = 0$ planes, and the remaining La and vacancies are accommodated at La2 sites in $z = 0.5$ planes (4i and 4j Wyckoff sites). Moreover, a small displacement of La ions from the center of the cubooctahedra cavities is detected. This shift is more important in the case of the La2 cations. In this phase, Ti atoms are also shifted from the center of the octahedra toward the vacancies-rich plane ($z = 0.5$)

(20) Varez, A.; Ibarra, J.; Rivera, A.; León, C.; Santamaría, J.; Laguna, M. A.; Sanjuán, M. L.; Sanz, J. *Chem. Mater.* **2003**, *15*, 225.

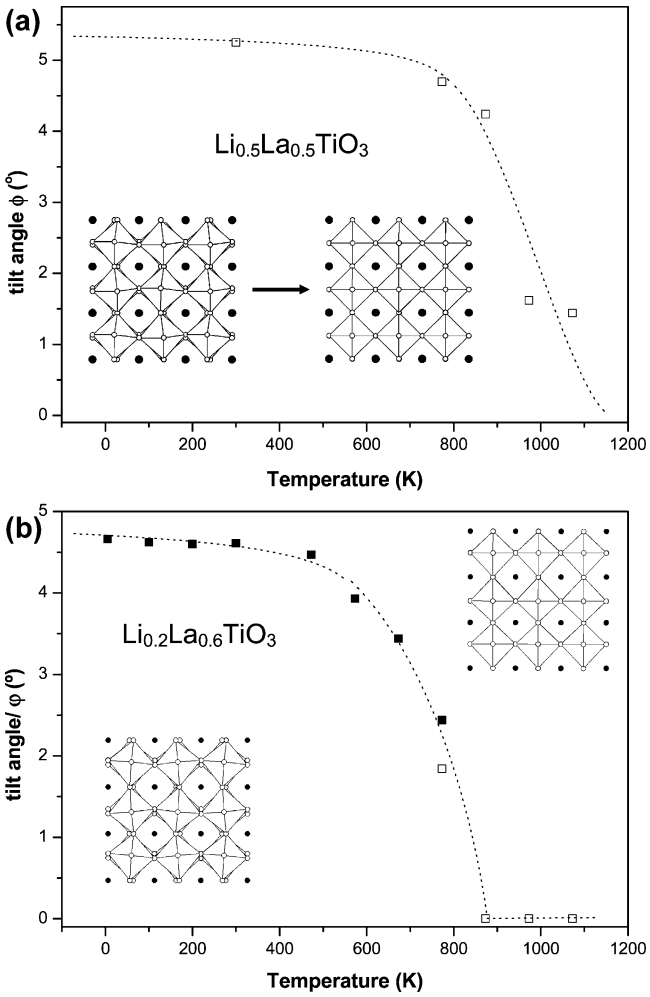

Figure 5. Evolution of the tilt angles with the temperature in (a) $Li_{0.5}La_{0.5}TiO_3$ and (b) $Li_{0.2}La_{0.6}TiO_3$ perovskites. Schematic views illustrating structures of four different phases analyzed are also displayed.

(Table 3). Finally, an antiphase tilting of TiO_6 octahedra was detected along the *b* axis ($a^0b^-c^0$ scheme in Glazer's notation).[21] As a consequence of the octahedra tilting, LaO_{12} cuboctahedra are considerably distorted and five different La−O distances are displayed in each polyhedra (Table 3).

The analysis of structural data obtained along the structural transition showed that coordinates of atoms in the orthorhombic phase approach those of the tetragonal one as the temperature increases above 873 K (Table 2 part a). Ti coordinates *x* and *z*, basically did not change during heating, but *y* coordinates of La1 and La2 sites approached 0.25 at 1073 K. A similar trend was deduced for oxygen atoms, where *z* coordinates of equatorial O2 and O3 oxygen come near to that of O4 oxygen ($z = 0.235$), and *x* coordinates of apical oxygens, O1 and O5, approached $x = 0.25$. The shift of La ions along the *b*-axis and the rotation of four oxygen atoms around this direction suggest that transformations produced have a displacive character. Along the orthorhombic−tetragonal transition, octahedral tilting is progressively eliminated (Figure 5a).

The ND pattern of the sample heated at 873 K was fitted with the tetragonal (a_p,a_p,$2a_p$) model (*P*4/*mmm* space group). Vacancy ordering and octahedral distortions detected in the orthorhombic phase were preserved in the tetragonal phase (see Table 2 part a). In this phase, the octahedral tilting was eliminated and distortions of La cubooctahedra became lower than detected in the orthorhombic sample (Table 3).

2. Rombohedral−Cubic Transformation. ND patterns of the quenched $Li_{0.5}La_{0.5}TiO_3$ perovskite, recorded at low temperatures, were fitted with the rhombohedral $\sqrt{2}a_p$,$\sqrt{2}a_p$, $2\sqrt{3}a_p$ model ($R\bar{3}c$ space group) given in Table 1. Structural analysis of the rhombohedral $Li_{0.5}La_{0.5}TiO_3$ sample showed that vacancy and La ions are randomly distributed in 6*a*-Wyckoff sites and Li ions occupy the center of unit cell faces of the ideal perovskite (18*d* Wyckoff sites).[16] In this perovskite, octahedra are out of phase tilted along the [111] direction ($a^-a^-a^-$ model in Glazer's notation)[21] (Figure 5b). In this phase, TiO_6 octahedra are regular (Ti−O distances ∼1.941 Å) but La cubooctahedra display considerable distortions (La−O distances between 2.56 and 2.90 Å) (see Table 4).

In the rhombohedral model, only *x* coordinates of oxygen atoms are variable. During thermal treatments, *x* coordinates remain constant up to 700 K; however, above this temperature this coordinate increased, approaching the characteristic value of the cubic phase, $x = 0.5$, at 1073 K. This change produced the progressive elimination of the octahedral tilting from 5 to 0°, detected along the [111] direction (Figure 5a).

In the case of the sample heated at 1073, the ND pattern was indexed with the cubic (a_p,a_p,a_p) model (*Pm*3*m* space group). In this structure TiO_6 octahedra are regular and distortions in LaO_{12} cubooctahedra are eliminated.

Discussion

During thermal treatment of $Li_{0.2}La_{0.6}TiO_3$ and $Li_{0.5}La_{0.5}TiO_3$ perovskites, two phase transitions have been detected. In the first sample, the orthorhombic−tetragonal transition, detected at 873 K, reduced the orthorhombic $2a_p$,$2a_p$,$2a_p$ unit cell to the tetragonal a_p,a_p,$2a_p$. In the second sample, the rhombohedral−cubic transition was detected at 1073 K; in this transition the rhombohedral $\sqrt{2}a_p$,$\sqrt{2}a_p$,$2\sqrt{3}a_p$ unit cell was transformed into the cubic a_p,a_p,a_p.

Comparative Study of Perovskite Structures. In orthorhombic perovskite, disposition of La^{3+} ions in alternated planes produced the shift of Ti toward the vacancy-rich planes ($z = 0.5$), giving two different Ti−O distances along the *c*-axis in TiO_6 octahedra (1.870 and 2.028 Å). The vacancy ordering produces the *c*-axis doubling detected in XRD and ND patterns. In the tetragonal phase, vacancy ordering and octahedral distortions were preserved.[6−8,19] In rhombohedral and cubic perovskites, distribution of vacancies is disordered and Ti^{4+} ions occupy the center of octahedra. Although in the rhombohedral perovskite a unique Ti−O distance is observed, a detailed observation of octahedra reveals the existence of a slight distortion along the *c*-axis. During the thermal treatment of this sample, the angle formed by Ti−O bonds with the *c*-axis changes from 55° to the ideal value (54.75°). This fact explains the expansion detected along the *c*-axis along the rhombohedral−cubic transition.[22,23]

(21) Glazer, A. M. *Acta Crystallogr. B* **1972**, *28*, 3384.

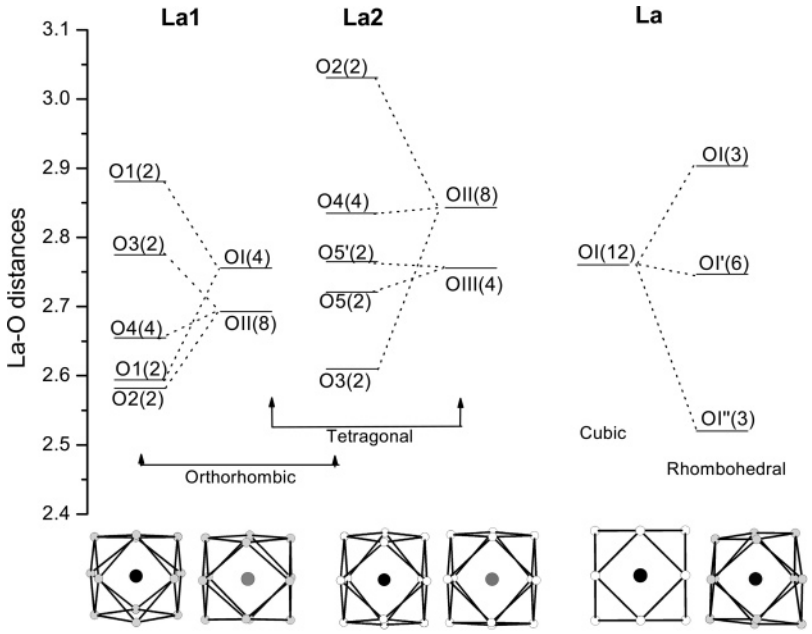

Figure 6. La−O distances in four analyzed phases. Along the orthorhombic−tetragonal transition, five La−O distances are transformed in two distances in $Li_{0.2}La_{0.6}TiO_3$ perovskite. Along the rhomboheral−cubic transition three La−O distances are converted in one distance in $Li_{0.5}La_{0.5}TiO_3$ perovskite. Schematic distortion of LaO_{12} cubooctahedra of different analyzed phases are also illustrated.

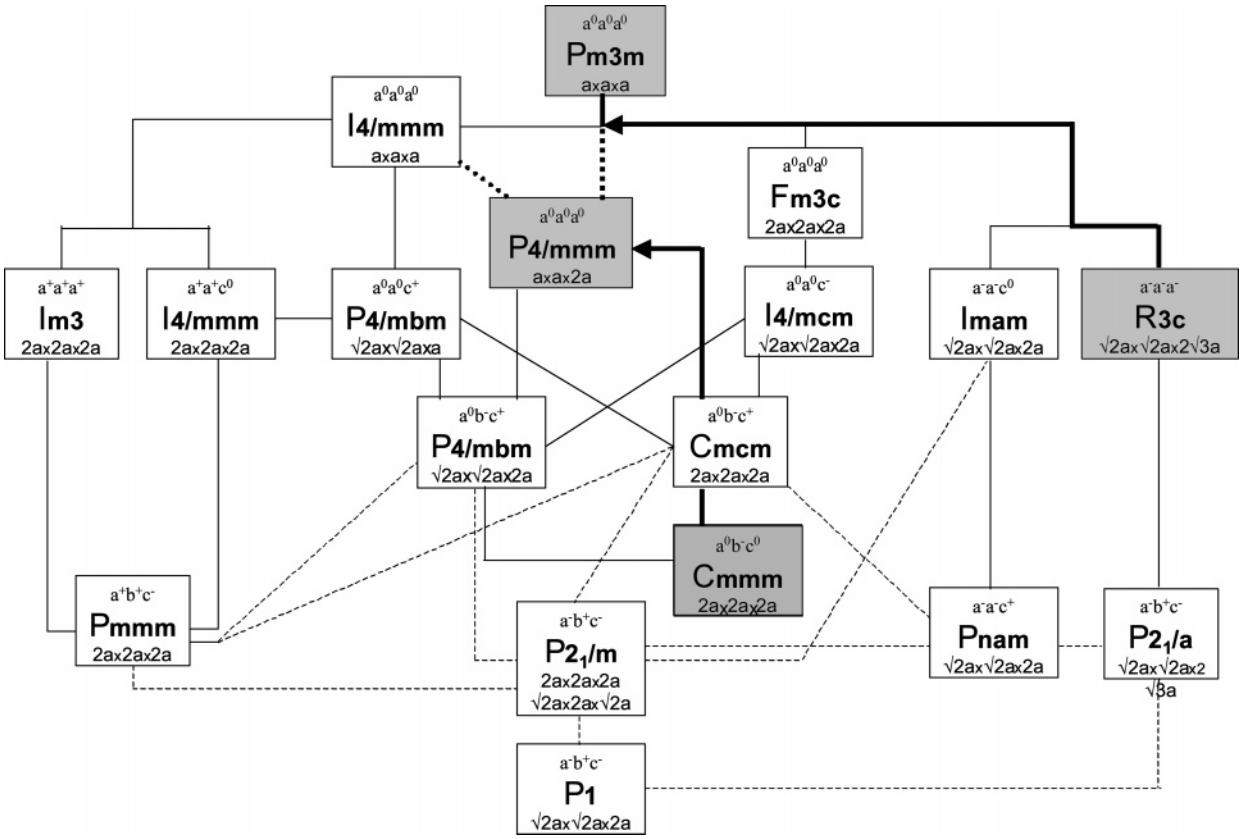

Figure 7. Schematic diagram illustrating the relationship between the space group symmetry and the octahedral tilting of the perovskites. In this diagram group/subgroup relations involved in phase transitions are indicated (Alexandrov's classification adopted).

To produce a better coordination of La cations, octahedra are tilted around specific axes, producing appreciable distortions in LaO_{12} cubooctahedra. In orthorhombic $Li_{0.2}La_{0.6}TiO_3$ phase, the anisotropic distribution of vacancies in alternated planes favors the octahedral tilting around the *b*-axis.[13−15,18] The presence of the octahedral tilting around the *b*-axis, the displacement of La ions along the *b*-axis, and the La-vacancy ordering along the *c*-axis justify the doubling of unit cell parameters along three axes. In the case of the rhombohedral $Li_{0.5}La_{0.5}TiO_3$ phase, octahedra are tilted along the [111] direction, producing a higher unit cell ($\sqrt{2}a_p$,$\sqrt{2}a_p$,$2\sqrt{3}a_p$).

(22) Varez, A.; Fernandez, M. T.; Sanz, J. *J. Solid State Chem.* **2004**, *177*, 4665.
(23) O'Keefe, M.; Hyde, B. G. *Acta Crystallogr. B* **1977**, *33*, 3802.

At increasing temperatures, LaO_{12} expansion is higher than that of TiO_6, causing a progressive decrease of the octahedral tilting in two perovskites. In tetragonal and cubic phases, the octahedral tilting is completely eliminated ($\varphi = 0$).

In the orthorhombic phase, La ions occupy sites with *m*2*m* symmetry and LaO_{12} cuboctahedra display important distortions. In La1 polyhedra, five La−O distances between 2.58 and 2.88 Å were detected, however, in La2 polyhedra these distances are between 2.61 and 3.03 Å (see Table 3 and Figure 6). In the case of tetragonal phase, La occupy sites with 4/*mmm* symmetry and distortions in LaO_{12} cubooctahedra are considerably reduced: in the case of La1 polyhedra, La−O distances are 2.69 and 2.75 Å, but in the case of La2 polyhedra, La−O distances are 2.75 and 2.84 Å. As a consequence of vacancy ordering, La cubooctahedra are alternatively flattened and elongated along the [001] direction (see Figures 5 and 6). In the rhombohedral phase, La occupy sites with *32* symmetry and cubooctahedra are considerably distorted, with three different distances (2.56, 2.75, and 2.96 Å). The elimination of the octahedral tilting makes that La occupy sites with *m*3*m* symmetry and La−O distances approach a unique value, 2.76 Å, in the cubic phase (see Figure 6).

On the other hand, the tilting of octahedra produces the distortion of square windows that connect contiguous A-sites of the perovskite.[13−16] In four analyzed phases, the number and dimensions of oxygen square windows are different. In the orthorhombic phase, the octahedral tilting makes it so that square windows perpendicular to the *a*-axis are less distorted (diagonal O−O distances = 3.88−4.14 Å) than those perpendicular to the *b*-axis (3.59−4.45 Å). In the tetragonal phase, square windows along *a* and *b* axes become equivalent.[19] In the case of the rhombohedral $Li_{0.5}La_{0.5}TiO_3$ perovskite, where La-vacancies are disordered, all square windows that connect contiguous A-sites display the same rhombic distortion, with diagonal O−O distances = 3.63 and 4.12 Å. In the cubic phase, square windows are regular and only one O−O distance is measured (3.85 Å). As a consequence of the vacancy distribution and the octahedral tilting detected, Li diffusion should be favored in alternated planes (2D mobility) in orthorhombic and tetragonal phases, but along three directions (3D mobility) in rhombohedral and cubic phases. Finally, the elimination of distortions in square windows favors Li motion in the cubic phase.

Structural Phase Transitions. During thermal treatment of perovskites, La−O distances increase more than Ti−O distances (0.6 and 0.07%). Different expansion of LaO_{12} and TiO_6 polyhedra favors the progressive elimination of octahedra tilting. The elimination of tilting was difficult to follow by XRD; in this sense, no apparent change was detected in high-temperature XRD patterns of the rhombohedral $Li_{0.5}La_{0.5}TiO_3$ perovskite.[20] From this fact, structural transformations produced during thermal treatment of samples must be analyzed with the ND technique.

In two analyzed samples, elimination of tilting drived a change of symmetry in the perovskite. In the case of $Li_{0.2}La_{0.6}TiO_3$, an orthorhombic−tetragonal phase transition was detected at 873 K; but, in the case of $Li_{0.5}La_{0.5}TiO_3$, a rhombohedral−cubic transformation was observed at 1073 K. In both cases, these transformations have a displacive character.

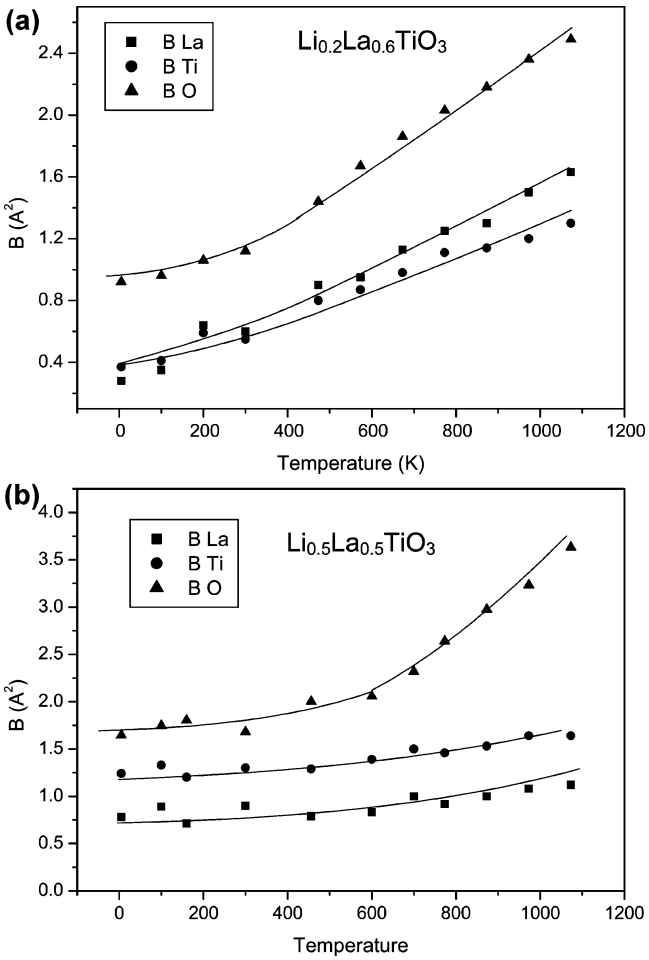

Figure 8. Evolution with temperature of oxygen, titanium, and lanthanum thermal factors for (a) orthorhombic $Li_{0.2}La_{0.6}TiO_3$ and (b) rhombohedral $Li_{0.5}La_{0.5}TiO_3$ perovskites. In both cases, two regimes with different local O mobility are detected.

Along the transitions, A-sites occupancy and octahedra distortions are not affected. From this fact, it is clear that vacancy ordering and octahedral tilting are not correlated and require different temperatures to be eliminated. To analyze possible transformations that relate tetragonal and rhombohedral phases, we have analyzed unit cells, octahedral tilting, and symmetry of perovskite phases on the basis of the Alexandrov's classification.[24] In the case of the orthorhombic perovskite, the elimination of octahedral tilting reduces unit cell volume by a factor of 4, but increases the symmetry from *Cmmm* to *P*4/*mmm*. In the case of the rhombohedral perovskite, unit cell volume is reduced by a factor of $4\sqrt{3}$, but symmetry changes from $R\bar{3}c$ to *Pm*3*m* (Figure 7). The elimination of vacancy ordering in the tetragonal *P*4/*mmm* phase should produce an additional reduction of unit cell volume (a factor of 2) and the increase of symmetry to *Pm*3*m*. However, to achieve this transition, migration of La ions is required, which demands temperatures near 1673 K.[11]

Finally, the evolution of atom thermal factors as a function of temperature is analyzed in Figure 8. In general, thermal

(24) Aleksandrov, K. S. *Kristallografiya* **1976**, *21* (*2*), 249.

factors increase with temperature; however, important differences have been observed in two analyzed samples. In the case of the rhombohedral phase thermal factors deduced are clearly higher than those determined in the orthorhombic phase, indicating that positional disorder is important in the rhombohedral phase.

In two analyzed phases, oxygen thermal factors are clearly higher than those of titanium and lanthanum ions; this observation suggests that some oscillation of octahedra around Ti cations could be activated during thermal treatment of samples. Taking into account that Li ions are preferentially located at square windows that relate contiguous A-sites, oscillation of octahedra should destabilize Li coordination, improving Li mobility. An analysis of the evolution of oxygen thermal factors in two analyzed perovskites suggests that octahedral oscillations could be produced in orthorhombic samples at lower temperatures than in tetragonal ones (400 and 600° C). However, the existence of an important positional disorder makes the detection of the crossover between the two regimes difficult to be observed in the rhombohedral phase.

Concluding Remarks

Structural analysis carried out with neutron diffraction in perovskites $Li_{3x}La_{2/3-x}TiO_3$, with $x = 0.06$ and 0.16, showed that vacancies are preferentially disposed in alternated planes of the orthorhombic Li-poor phase, but completely disordered in the rhombohedral Li-rich phase. To achieve a better coordination of La ions, octahedra are out-of -phase tilted along the *b*-axis in orthorhombic phase and along the [111] direction in the rhombohedral phase ($a^0b^-c^0$ and $a^-a^-a^-$ schemes in Glazer's notation).

Thermal treatment of perovskites produces the elimination of the octahedral tilting. This elimination causes the transformation of the orthorhombic into the tetragonal phase and the rhombohedral into the cubic phase. In both cases, distribution of La and vacancies was preserved, indicating that temperatures higher than 1073 K are required to induce the vacancy disordering. In this sense, quenching treatments from 1673 K into liquid N_2 are necessary to prepare disordered perovskites.

Both structural features, namely, the octahedral tilting and the vacancies ordering, are the main characteristics that differentiate the analyzed phases. Vacancy ordering detected in orthorhombic $Li_{0.2}La_{0.6}TiO_3$ perovskite explains the preferential motion of lithium in alternated planes. This type of motion contrasts with the three-dimensional one, detected in the rhombohedral $Li_{0.5}La_{0.5}TiO_3$ perovskite.

Acknowledgment. We thank C. León and J. Santamaría for helpful discussions and ILL for the provision of neutron beam time. We thank also the Spanish CICYT (MAT2001-3713-C04-03 and MAT2004-03070-C05-02 projects) for financial support.

CM047841F